cient is meaningless without including at least the following details: For weakly absorbing materials a list of impurity concentrations is needed, not just the commonly quoted minimum purity. Similarly, sufficient details of the wavelength distribution must be given. Finally, information regarding the form of the absorber (single crystal or polycrystalline) and the measuring geometry are necessary to estimate the effect of scattering.

ACKNOWLEDGMENTS

The authors are greatly indebted to Dr. D. R. Chipman and Dr. L. D. Jennings for many helpful comments regarding this work.

*National Research Council Postdoctoral Research Associate. Permanent address: Department of Physics, University of Helsinki, Siltavuorenpenger 20 C, Helsinki 17, Finland.

[1]R. W. James, *Optical Principals of the Diffraction of X-Rays* (G. Bell, London, 1958), p. 51.
[2]P. L. La Fleur, Acta Cryst. A26, 674 (1970).
[3]B. E. Warren, Acta Cryst. 6, 803 (1953).
[4]R. J. Weiss, *X-Ray Determination of Electron Distributions* (North-Holland, Amsterdam, 1966), pp. 20, 21.
[5]W. J. Veigele, P. T. Tracy, and E. M. Henry, Am. J. Phys. 34, 1116 (1966).
[6]*International Tables for X-ray Crystallography* (Kynoch Press, Birmingham, England, 1962), Vol. III, p. 161.
[7]D. R. Chipman, Acta Cryst. A25, 209 (1969).
[8]D. R. Chipman, J. Appl. Phys. 26, 1387 (1955).
[9]P. M. de Wolff, Physica XIII, 62 (1947).
[10]R. J. Harrison and A. Paskin, Acta Cryst. 17, 325 (1964).
[11]A. J. Dearden, J. Appl. Phys. 37, 1681 (1966).
[12]D. T. Keating and J. J. Antal, J. Appl. Phys. 26, 1041 (1955).

PHYSICAL REVIEW B VOLUME 4, NUMBER 4 15 AUGUST 1971

Fermi Surface of Antimony: Radio-Frequency Size Effect*

R. A. Herrod, C. A. Gage, and R. G. Goodrich
Department of Physics and Astronomy, Louisiana State University, Baton Rouge, Louisiana 70803
(Received 12 March 1971)

Radio-frequency size-effect measurements have been performed on high-purity single-crystal antimony plates approximately 0.15–0.36 mm thick. Extremal calipers of the Fermi surface which were obtained from the data were fit in an internally consistent manner to a Fermi-surface model consisting of three electron pockets and three sets of doubly degenerate hole pockets. The tilt angles and shapes of the pockets basically confirm the general features of the Fermi-surface model arising from a previous pseudopotential calculation. The sizes of the pockets, however, differ somewhat from the predictions. Comparisons between the present data and previous de Haas–van Alphen and ultrasonic geometric-resonance measurements are made.

I. INTRODUCTION

In the past, the Fermi surface (FS) of antimony has been investigated through several experimental techniques. They include the galvanomagnetic effect,[1,2] ultrasonic attenuation,[3–6] de Haas-Shubnikov effect,[7,8] cyclotron resonance,[9] and the de Haas–van Alphen (dHvA) effect.[10–13] The interpretation of these experiments was confusing and often in conflict until an energy-band calculation by Falicov and Lin (FL)[14] was performed. In this calculation FL showed that (a) there are three electron pockets and six hole pockets and (b) the electrons are located at the L point in the Brillouin zone (BZ) while the hole pockets are in the mirror plane at the point H in the BZ (Fig. 1). While this calculation resolved the situation concerning the sign of the carriers, number of pockets of each, and their location in the BZ, it did not have sufficient accuracy to predict the detailed shapes of these pieces of the FS. The data which are re-

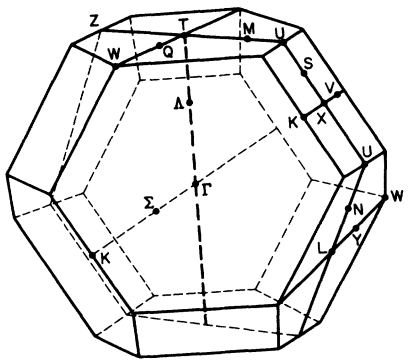

FIG. 1. The BZ for Sb.

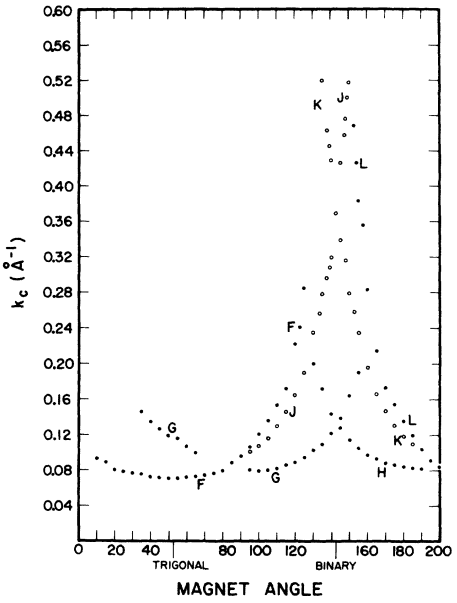

FIG. 2. Caliper values, in Å^{-1}, and direction for $\vec{n}$ parallel to bisectrix axis.

ported here give the details of the dimensions of the FS and should allow a refinement of the band-structure calculation to be performed.

The determination of FS dimensions using the radio-frequency size effect (rfse) has been described earlier.[15, 16] Briefly, the experiment consists of measuring the rf surface impedance (R) of a thin single-crystal plate as a function of magnetic field applied in the plane of the plate. Discontinuities in the surface impedance are exhibited when the strength of the magnetic field is such that extremal electronic orbits on the FS exactly span the sample thickness. The extremal FS dimensions are then obtained from the integration of the Lorentz equation with respect to time. This gives values of the extremal dimensions of the FS to be $k_c = 0.015\,194Hd$, where H is the value of the applied field in G, d is the sample thickness in mm, and k_c is the FS extremal dimension in Å^{-1}.

In the sections which follow, the important aspects of the experimental techniques are described, and the experimental results, data analysis, and caliper assignments are given.

II. EXPERIMENTAL PROCEDURE

A zone-refined bar of Sb (quoted purity: 99.9999%) was obtained from Cominco Products, Incorporated. The Sb bar contained crystals of sufficient size that further crystal growth was unnecessary. After orienting the selected crystals, thin slabs were cut out by spark erosion. The general technique for rfse sample preparation has been described in detail in Ref. 15. After spark planing, the samples were lapped in a solution containing equal parts of acetic, hydrofluoric, and nitric acids and water in order to remove the surface strain resulting from the thinning process.

The finished samples were always checked to assure that the final orientation was within ± 0.5° of the desired direction. The final sample thicknesses were typically between 0.15 and 0.36 mm. Samples this thin were used in order to make the small calipers obtained occur at reasonable field values. A single preformed tank coil was used throughout the experiment. The sample thickness was determined by measuring the area of the face and weighing it in the manner described in Ref. 15. The rfse signals were detected using the apparatus described in Ref. 16. Both the first and second derivatives of the real part of the surface impedance vs magnetic field can be recorded with this apparatus. The electronic system and sample thickness measuring techniques give an over-all reproducibility to the caliper values of 0.006 Å^{-1}, determined by comparing the caliper values on different samples. All of the measurements were performed at 1.2 °K using a rf frequency of 9 MHz in magnetic fields ranging between 10 and 200 G.

III. EXPERIMENTAL RESULTS

Data were obtained for field rotations in three planes. Samples were used having the normal $\vec{n}$ to the face of the slab parallel to the binary and bisectrix axes and to an axis rotated 7° from the trigonal axis toward the bisectrix axis away from

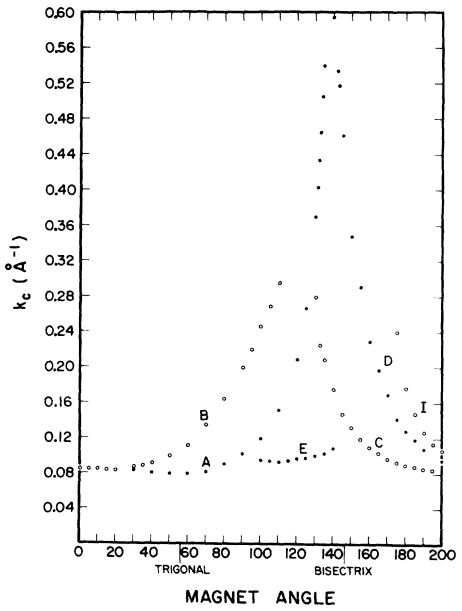

FIG. 3. Caliper values, in Å^{-1}, and direction for $\vec{n}$ parallel to binary axis.

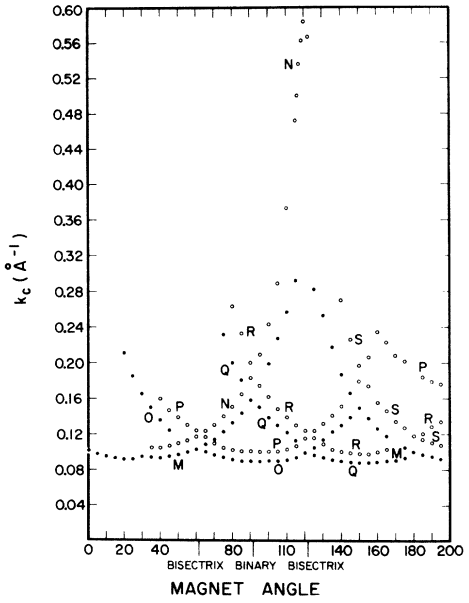

FIG. 4. Caliper values, in Å^{-1}, and direction for $\vec{n}$ 7° off the trigonal axis towards the bisectrix axis away from ΓX.

ΓX. The last orientation was chosen because thin samples with $\vec{n}$ parallel to the trigonal axes failed to produce rfse signals. A probable reason for the inability to detect signals in this orientation is that the thin plates may "peel" during the cool-down process because of the close orientation to the easily cleaved bisectrix binary plane. Also, an axis 7° from the trigonal towards the bisectrix axis was chosen because of the geometry of the electron pockets determined from data taken in the other two orientations. The resulting FS calipers for $\vec{n}$ along the binary and bisectrix axes and 7° from the trigonal axis are shown in Figs. 2–4, respectively. The calipers which could be definitely assigned as being due to the addition of two orbits are not shown in these figures. Signals attributable to the addition of as many as five orbits were seen.

The rfse line shapes observed in Sb display the same general characteristics observed earlier in Cd,[15] Zn,[16] and Tl.[17] The signal-to-noise ratio in samples with $\vec{n}$ directed 7° off the trigonal axis was higher than that observed in the above three metals. Signals observed from samples having $\vec{n}$ parallel to the other two symmetry axes also exhibited high signal-to-noise ratios. The signal strength decreased rapidly with angle as the turning points of the pockets were approached. Since at these points the electrons spend very little time in the skin depth, their effect on the change in surface impedance is small. Signal strengths decreased slowly with increasing temperature with signals associated with the minimal calipers for H parallel to the electron pocket axis clearly visible at 4.2 °K.

All of the caliper values reported here were calculated by choosing the point in field of maximum slope preceding the first major peak in the rfse line shape obtained on a plot of the derivative of the real part of the surface impedance with respect to magnetic field (dR/dH). This point corresponds to the first peak in the second derivative curve (d^2R/dH^2). This has been shown to be a reliable point on the line shape from which to compute the caliper value in past rfse experiments devoted to FS determinations.[15–17] In angular regions where several caliper series are present and the rfse lines overlap, a slightly different procedure was used to determine the caliper point on each line. It was observed that the difference in field values between peaks (ΔH) on the second derivative curves was a constant for a given line. In Fig. 5, a recorder tracing of d^2R/dH^2 vs H taken with H applied 20° from the bisectrix direction in an $\vec{n}$ 7° off the trigonal axis sample is shown. The line shapes associated with series M, O, P, Q, and S are shown in this plot. It is seen that ΔH is a constant for each line and the caliper point can be determined by extrapolating to the first peak in the line shape. This procedure was applied even when the first peak in the second derivative was visible. In these latter cases, the agreement between the extrapolated position of the first peak and the measured position agreed to within the measuring accuracy. The experimental error in the determination of the calipers by this method is ±0.006 Å^{-1}. This accuracy was checked by comparing the caliper values obtained from different samples for the

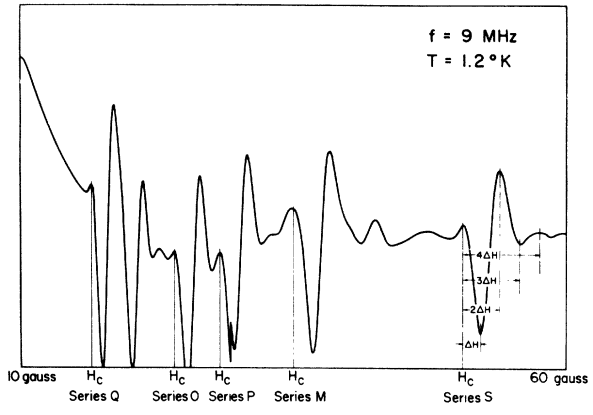

FIG. 5. Second-derivative recorder tracing for $\vec{n}$ 7° off the trigonal axis towards the bisectrix axis showing the caliper peaks for series Q, O, P, M, and S. The line shape associated with series S shows the extrapolation method of locating the field, H_c, associated with the caliper. H_{dc} directed 20° from bisectrix.

same orbit and by comparing the determination of points on the FS obtained from different sample orientations. These independent determinations always agreed to within the quoted accuracy. This point on the line has also been shown to be the caliper point for cylindrical FS's in a recent calculation of line shapes by Juras.[18] Further support for the choice of this point on the line as the caliper point has recently been given by Boudreau and Goodrich[19] from the line-shape studies on Cd.

IV. DATA ANALYSIS AND CALIPER ASSIGNMENT

In the following discussion, the term caliper will be defined as a vector quantity in $\vec{k}$ space which is the direction of $\pm\hat{n}\times\hat{H}$ and has a magnitude equal to the length of the line segment formed by projecting an external orbit (in $\vec{k}$ space) onto a plane perpendicular to $\hat{n}$. Since rfse always obtains values of extremal (maximum or minimum length) calipers, the term caliper will be taken to mean an extremal caliper throughout the remainder of this paper.

Since the electron pockets are centered at the L point in the BZ, they must exhibit inversion symmetry through the L point. Calipers arising from the electrons then could be plotted with their midpoint at L for the $\hat{n}$ parallel to binary data. That is, all of the calipers for the electrons in this orientation are due to central orbits. On the other hand, the hole pockets are located at a general point in a mirror plane and do not exhibit inversion symmetry. Therefore, the assignment of calipers to these pockets cannot be done unambiguously. In order to be consistent, we have assigned all of the calipers of the hole pockets as if they arose from central orbits. As will be seen in what follows, this leads only to a small error in the dimension obtained.

The extremal areas for some of the outlines obtained from the data were computed. Both polar planimeter measurements and direct computation of the areas using Simpson's rule were made in each case and were found to agree with each other to better than 1%.

A. Bisectrix Plane

In the bisectrix plane, calipers were assigned to the two electron pockets which when projected onto the bisectrix plane cross at the binary axis and to two rather distorted hole pockets also crossing at the binary axis. Figure 6 is a plot of the caliper points in this plane. Caliper series K was assigned to the curved side of one electron pocket while series J formed the curved side of the other one. Series F was then assigned to the flat side of the electron pocket bounded by series K while series L formed the flat side of the pocket bounded by series J. The projection of these electron pockets have their axes 8.3° on either side of the binary

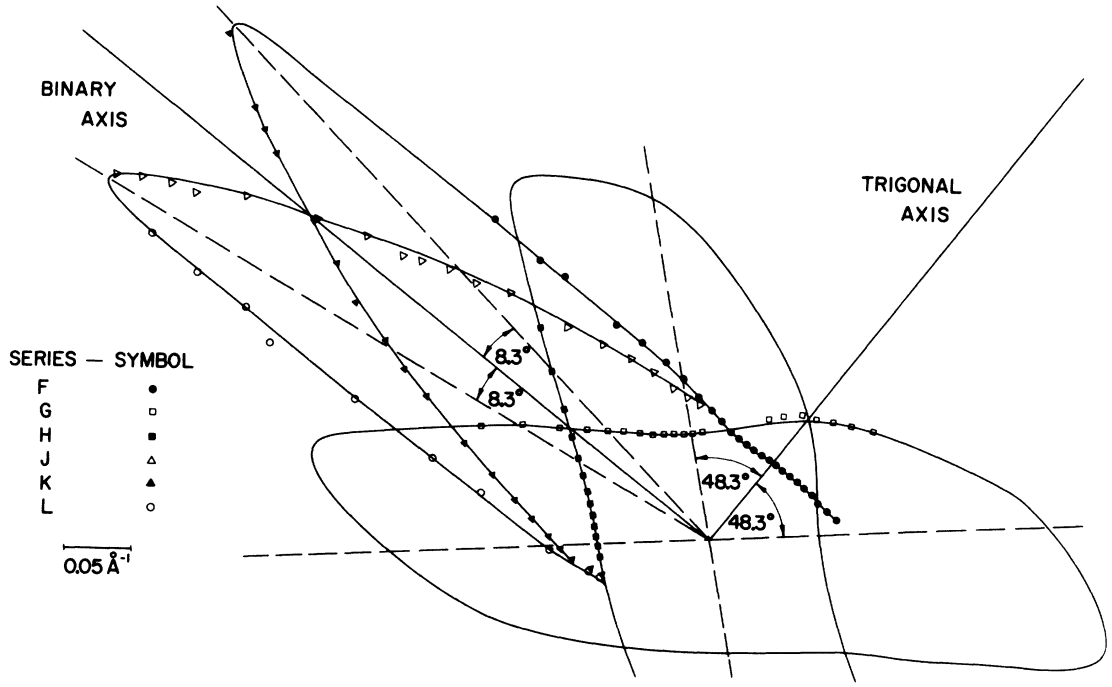

FIG. 6. Projection of two electron pockets (series J, L, F, and K) and two hole pockets (series G and H) of Sb onto the bisectrix plane.

axis and have a length of 0.518 $Å^{-1}$ and a width perpendicular to this axis of 0.075 $Å^{-1}$. As will be discussed later, the curvature of these electron pockets with respect to the binary axis aided in assigning calipers in the binary plane.

The signals produced by these electrons were very strong. Line shapes were observed over most of the angular region resulting from the addition of up to five orbits. These strong harmonic series crossed over other weaker series, prematurely terminating them or masking them altogether. The intensity of the rfse peaks is, to a large extent, dependent upon the geometry of the orbit. That is, extremal orbits that spend proportionately longer time in the skin depth of the sample, and whose trajectories are parallel to the surface while in the skin depth, have a greater effect on the surface impedance than do extremal orbits calipered at more pointed segments of the FS. An example of the result of these effects is the termination of series F 15° before the turning point of the electron pocket. As the FS gets rapidly more pointed in this region, one of the orbit addition series associated with series J crosses over and masks the weakened line. The third electron pocket which should have been seen in an almost end-on fashion in this orientation was entirely masked by the harmonic series occurring in the region. A probable explanation for the lack of strong signals from this type of orbit is that the carriers are almost parallel to the surface during most of their trajectory in the sample. That is, the carriers simultaneously produce changes in the impedance as if the orbits were exactly spanning the sample, spanning the sample at one, two, etc., skin depths. This would produce a cancelling effect in the rfse line shape resulting in very weak signals. The observed shape and the symmetry requirements for the electron pockets suggest that the central polar plots of the caliper series result in a very representative cross section for these pieces of the FS.

Only two caliper series were observed in this orientation which could be assigned to hole pockets of the FS. Series G was observed over a 120° angular region before being hidden by the stronger electron signals of series K and L and the harmonic signals of series F. Series G was assigned to one side of a hole pocket having an axis of minimum caliper of 48.3° on one side of the trigonal axis. Series H was assigned to one side of another hole pocket having an axis of minimum caliper 48.3° on the other side of the trigonal axis. This pocket's orientation was such that series H could be followed for only 60° before series L and K on one side and series F and J on the other side interfered. The third hole pocket expected in this orientation was not seen. The two observed series associated with the hole pockets yield a fairly complete outline of the shape of these pieces of the FS. The shape and value of the turning points of these hole pockets were deduced from caliper values in the trigonal plane.

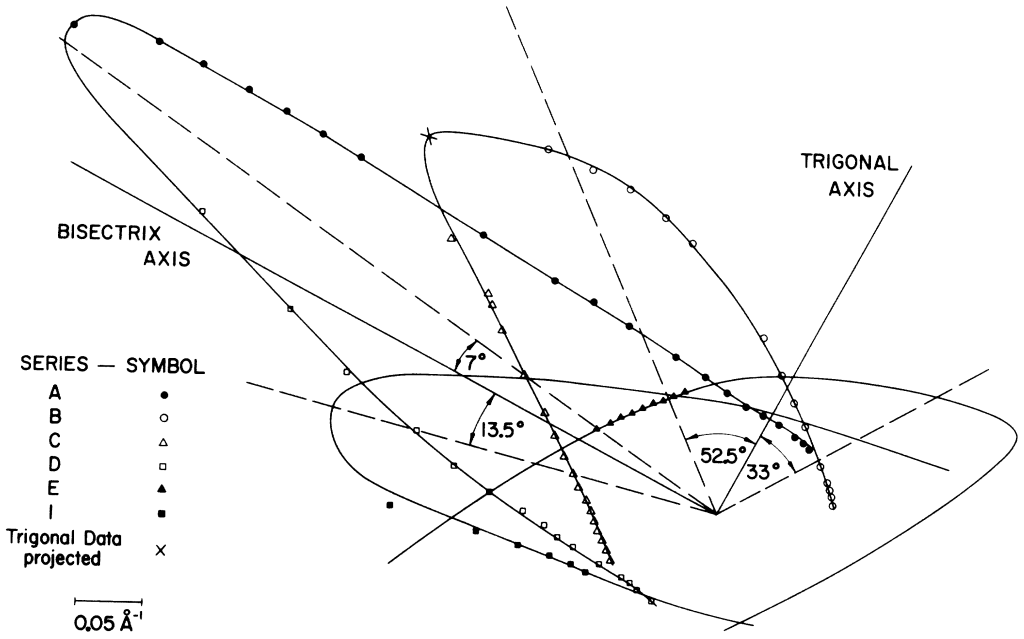

FIG. 7. The electron pocket (series A and D) and hole pocket (B and C) of Sb lying in the binary plane. Also shown are the out-of-plane electron pocket (series I) and hole pocket (series E) projected onto this plane. The point X is the maximum caliper for the binary plane hole pocket projected onto this plane from a plane having $\tilde{n}$ 7° off the trigonal axis.

TABLE I. Comparison of dHvA areas. Extremal areas in Å^{-2}.

Field direction	Type pocket	Present data	Windmiller[a]
Binary	Electron	0.0364	0.0343
7° from trigonal towards bisectrix	Electron	0.0425	0.0413
Binary	Hole	0.0214	0.0205
31° from trigonal towards bisectrix	Hole	0.0204	0.0188

[a]See Ref. 13.

B. Binary Plane

Figure 7 shows a plot of the caliper points in the binary plane. At least parts of all four pockets expected in this orientation were seen. Series *A* was assigned to the relatively flat side of the in-plane electron pocket while series *D* was assigned to the curved side. The maximum length of this pocket is 0.594 Å^{-1} with its width being 0.080 Å^{-1}. The axis of the electron pocket lies 7° off the bisectrix axis towards the trigonal axis. The dHvA area of this pocket was computed directly from the measured calipers and is compared with the area of Windmiller[13] in Table I. The 6.2% difference in the two values is not too surprising since the claimed measuring accuracy of 0.006 Å^{-1} becomes quite significant in the regions of very small caliper values. It was originally thought that the actual caliper peak in the d^2R/dH^2 curves was being consistently washed out. Assuming this, new caliper values were assigned by extrapolating back another ΔH. This procedure led to internal inconsistencies as well as to a dHvA area 5.5% too small. Attempts were then made to determine a constant scaling factor for the caliper values which would leave all the pockets internally consistent and yield closer agreement with the dHvA data. This procedure also failed to satisfy both requirements. Since the original caliper values at least provided complete internal agreement from one orientation

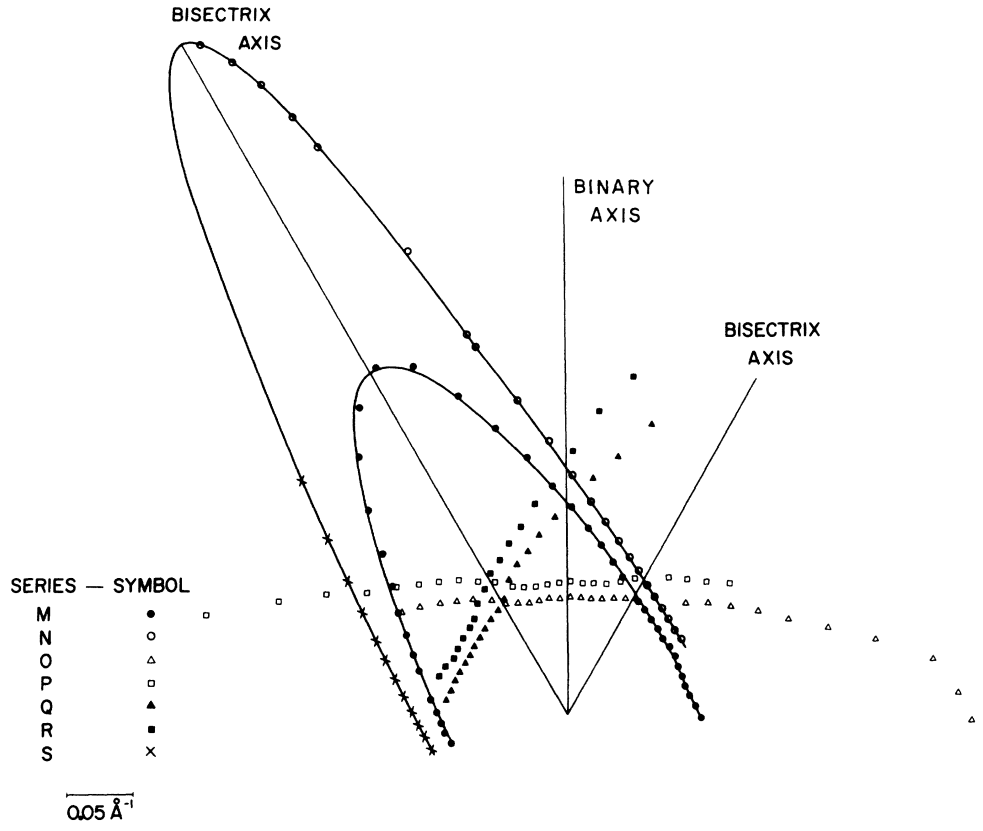

FIG. 8. The electron pocket (series *N* and *S*) lying in a plane having $\vec{n}$ 7° off the trigonal axis towards the bisectrix axis. Series *M* is the projection of a hole pocket onto this plane. Projections of parts of two other electron pockets (series *P* and *R*) and two other hole pockets (*O* and *Q*) onto this plane.

to another, these values have been used.

Series *I* was assigned to one side of the electron pocket not lying in the binary plane. Other caliper points for this pocket were completely hidden by the much stronger in-plane electron series as well as the hole series in this orientation. The axis of this electron pocket projects onto the binary plane 13.5° from the bisectrix axis on the side opposite the main electron pocket. Series *C* and *B* are assigned to the in-plane hole pocket. The axis of minimum caliper lies 52.5° off the trigonal axis towards the bisectrix axis. This is in excellent agreement with the dHvA observed minimum area axis of 53.0° from trigonal. These caliper series, as mentioned previously, were plotted as if they were arising from central orbits. The dHvA area calculated from these calipers is also compared with that of Windmiller in Table I. The percent difference is comparable to that of the electron pocket. Thus, the use of central calipers for this pocket has only a small effect. Series *E* was assigned to the out-of-plane hole pocket. This series could be followed for only 40° before being lost in the much stronger series *A*, *D*, and *C*. The axis of minimum caliper projects onto this plane at an angle of 33° from the trigonal axis on the side opposite the main hole pocket, which agrees with that value obtained by projecting the in-plane axis 60° out of this plane. The shapes of the hole pockets near the turning points were drawn in using caliper values obtained in the trigonal sample.

The calipers assigned in the bisectrix plane and binary plane give a model which shows good internal consistency. The extremal dimension of the main electron pocket in the binary plane is 0.594 Å^{-1}. When projected back onto the bisectrix plane its value of 0.514 Å^{-1} is in excellent agreement with the measured dimension of 0.518 Å^{-1}. The shape and axis direction of the holes are consistent in these two planes also.

C. 7° Off-Trigonal Plane

For the sample with $\hat{n}$ 7° from the trigonal axis towards the bisectrix axis, signals were observed which could be attributed to three electron and three sets of doubly degenerate hole pockets. The calipers are shown plotted in Fig. 8. Series *N* and *S* were assigned to the electron pocket lying in the plane of the sample. This pocket has an extremal length of 0.594 Å^{-1}, in excellent agreement with the lengths found in the other planes. The caliper points on one side of the axis when folded over lie along the caliper points on the other side showing the symmetry of the pocket. The dHvA area computed for this pocket is 3% larger than that measured by Windmiller. Series *P* and *R* were assigned to the two electron pockets not

TABLE II. Comparison of maximum and minimum caliper values.

$\hat{n}$ ∥	Type carrier	Minimum and maximum caliper (Å^{-1}) Eckstein[a]	KW[b]	KM[c]	EBH[d]	This experiment[e]	FL[f]
Trigonal	Holes			(0.075) (0.305)		0.092 0.302	
	Electrons	0.086			0.095 0.458		
	Holes			(0.092) (0.568)		0.105 0.594	
				0.091 0.341	0.083	0.084 (0.350)	0.069(0.068) 0.413(0.486)
Binary		0.067					
	Electrons		0.083 0.499	0.085 0.596	0.076 0.489	0.080 0.594	0.061(0.072) 0.398(0.424)
	Holes			(0.085)		0.080 (0.301)	
Bisectrix	Electrons	0.081					
				(0.085)		0.075 0.518	

[a]See Ref. 3. No assignment to electrons on holes was made by this author.
[b]See Ref. 20. These results were obtained by inversion of dHvA data for a nonellipsoidal FS.
[c]See Ref. 6. Bracketed values taken from graphs (±10%). Other numbers are the quoted values.
[d]See Ref. 4. No assignment to electrons or holes was made by these authors.
[e]Bracketed calipers are obtained by projection from data from the other orientations. The trigonal orientation is data from the $\hat{n}$ parallel to 7° from the trigonal towards the bisectrix away from TX. All values are ±0.006.
[f]See Ref. 14. Bracketed values obtained from the present calculation and unbracketed were measured from the graphs of FL.

TABLE III. Comparison of tilt angles in binary plane. Axis angle for minimum area from trigonal axis towards bisectrix axis.

Pocket	FL[a]	Windmiller[b]	Present experiment[c]
Holes	41.0°	53.0±0.1	52.5±0.5
Electrons	83.0°	84.0±0.3	83.0±0.5

[a]See Ref. 14.
[b]See Ref. 13.
[c]Field direction for minimum caliper.

lying in the plane of the sample.

Series M was assigned to the hole pocket which projects onto this plane along the axis of the main electron pocket. Projecting the extremal length of this hole back onto the binary plane perpendicular to the minimum caliper direction yields 0.350 $Å^{-1}$ and is shown in Fig. 7. The shape near the turning point in the binary plane is not known but a continuation of the measured curvature in the turning-point region has been drawn in. Since this hole pocket is ellipsoidal in the 7° off-trigonal plane, a rough estimate can be made of its area $= \pi ab$. This area of 0.0204 is 8.5% larger than that measured by Windmiller. Series Q and O were then assigned to the other two hole pockets observed in this orientation.

V. CONCLUSION

The shape and size of the FS proposed here show excellent internal agreement in caliper values and tilt angles. The tilt angles measured in this experiment agree with those measured by Windmiller. The dHvA areas computed from the data are consistently larger than those measured by Windmiller. The uncertainty in the measured caliper values is 0.006 $Å^{-1}$, as determined by the reproducibility from sample to sample and the internal agreement shown between orientations. This uncertainty inherent in the rfse experiment introduces a very small percentage error in measurements on the fairly large FS's of metals but the error becomes as large as 8% for the small calipers of the FS encountered in Sb. In addition, the low carrier concentration in Sb ($\sim 10^{19}/cm^3$) causes the skin depth δ at rf frequencies to be at least a factor of 10 larger than in normal metals. This could cause a shift in the observed rfse lines because the condition for the rfse that $\delta/d \ll 1$ is not well satisfied.

In general, good agreement between this experiment and the pseudopotential calculation of FL is exhibited for type, number, and tilt angle of the FS pockets. In order to make direct comparisons of the present data to the model obtained by FL, the pseudopotential and Fermi energy used by FL were used to recalculate the FS at approximately 40 points on the electron surface and 40 points on the hole surface. Eighty-nine plane waves were used in the expansion and the accuracy of the present calculation was checked at symmetry points in the BZ and found to agree with the values quoted by FL to three significant figures. Table II is a comparison of extremal caliper values for the FS of Sb between this experiment and others and the results of FL. The discrepancy in caliper values between the experiments and the calculations of FL is not surprising since a slight shift in the Fermi energy changes the dimensions of the calculated FS drastically. Table III is a comparison of the tilt angles obtained by Windmiller and FL with those measured in this experiment.

ACKNOWLEDGMENTS

The authors gratefully acknowledge many helpful discussions with Professor C. G. Grenier during the course of the analysis of this experiment. One of the authors (R. A. H.) wishes to acknowledge assistance from the Dr. Charles E. Coates Memorial Fund of the L. S. U. Foundation, donated by George H. Coates, for assistance in the publication of this manuscript.

*Work supported by the National Science Foundation, Grant No. GP-11008.

[1]S. J. Freedman and H. J. Juretschke, Phys. Rev. 124, 1379 (1961).
[2]S. Epstein and H. J. Juretschke, Phys. Rev. 129, 1148 (1963).
[3]Y. Eckstein, Phys. Rev. 129, 12 (1963).
[4]L. Eriksson, O. Beckman, and S. Hornfeldt, J. Phys. Chem. Solids 25, 1339 (1964).
[5]J. B. Ketterson, Phys. Rev. 129, 18 (1963).
[6]A. P. Korolyuk and L. Ya. Matsakov, Zh. Eksperim. i Teor. Fiz. 52, 415 (1967) [Sov. Phys. JETP 25, 270 (1967)].
[7]G. N. Rao, N. H. Zebouni, C. G. Grenier, and J. M. Reynolds, Phys. Rev. 133, A141 (1964).
[8]L. S. Lerner and P. C. Eastman, Can. J. Phys. 41, 1523 (1963).
[9]W. R. Datars and J. Vanderkooy, IBM J. Res. Develop. 8, 247 (1964).
[10]D. Shoenberg, Phil. Trans. Roy. Soc. London A245, 1 (1952).
[11]Y. Saito, J. Phys. Soc. Japan 18, 452 (1963).
[12]M. H. Halloran, F. F. Huppe, and R. N. Dexter, Bull. Am. Phys. Soc. 8, 517 (1963).
[13]L. R. Windmiller, Phys. Rev. 149, 472 (1966); and L. R. Windmiller and M. G. Priestley, Solid State Commun. 3, 199 (1965).
[14]L. M. Falicov and P. J. Lin, Phys. Rev. 141, 562 (1966).
[15]R. C. Jones, R. G. Goodrich, and L. M. Falicov, Phys. Rev. 174, 672 (1968).
[16]O. L. Steenhaut and R. G. Goodrich, Phys. Rev. B

1, 4511 (1970).
[17]C. A. Gage and R. G. Goodrich, Phys. Rev. B 3, 3214 (1971).
[18]G. E. Juras, Phys. Rev. B 2, 2869 (1970).
[19]D. A. Boudreau and R. G. Goodrich, Phys. Rev. B 3, 3086 (1971).
[20]J. B. Ketterson and L. R. Windmiller, Phys. Rev. B 1, 463 (1970).

PHYSICAL REVIEW B VOLUME 4, NUMBER 4 15 AUGUST 1971

Diffuse Scattering from Defect Clusters near Bragg Reflections*

P. H. Dederichs†
Solid State Division, Oak Ridge National Laboratory, Oak Ridge, Tennessee 37830
(Received 25 February 1971)

The diffuse scattering from crystals containing defect clusters with strong displacement fields has been calculated. The scattering is extremely large and concentrated in small regions near the Bragg reflections. For small concentrations the diffuse intensity is essentially determined by a "cluster form factor" depending explicitly on the displacement field. The scattering is studied in detail for small and large deviations from the Bragg reflection. Exact expressions are given for the moments of the scattering, depending sensitively on the displacement field in the core of the cluster. The diffuse scattering for strong displacement fields shows a pronounced asymmetry; its center does not coincide with the position of the Bragg peak, in agreement with recent experimental observations.

I. INTRODUCTION

The diffuse scattering from crystals containing defects with displacement fields was first considered by Eckstein[1] and Huang.[2] This theory has been worked out in more detail by Cochran and Kartha[3,4] and by Borie,[5] and has also been the subject of a recent paper of Keating[6] which has generated some controversy.[7] A number of excellent papers about diffuse scattering of defects have been published by Krivoglaz and co-workers,[8,9] but they seem to have been widely overlooked.

The diffuse scattering from defect clusters has also been considered by Krivoglaz and Ryaboshapka,[10] who calculated the scattering from dislocation loops. According to them, the diffuse scattering from loops is extremely large near the Bragg reflections and, under certain conditions, the center of the diffuse scattering can be displaced from the position of the Bragg peak.

Recently the diffuse scattering from defect clusters has been observed experimentally.[11–16] The present author's observation of the diffuse scattering of dislocation loops in neutron-irradiated Cu crystals has been the reason to consider the scattering from defect clusters in somewhat more detail.

II. GENERAL FORMULAS FOR THE DIFFUSE SCATTERING

In this section we derive the general formulas for the elastic scattering from lattices with defects. In the following we are mainly interested in defects with strong displacement fields. Such large displacements are typical for defect clusters rather than isolated point defects; e.g., for a dislocation loop the characteristic displacement is a Burgers vector or a lattice constant. The method we use is essentially that of Krivoglaz[8,9] except that we consider the image field explicitly. For simplicity we take only the scattering at the displaced matrix atoms into account, since this is the only important contribution near the Bragg reflection. The diffuse intensity is given by the scattering function:

$$S(\vec{K}) = \sum_{m,m'} e^{i\vec{K}\cdot(\vec{R}^m-\vec{R}^{m'})} \times \left(\langle e^{i\vec{K}\cdot(\vec{u}^m-\vec{u}^{m'})}\rangle - \langle e^{i\vec{K}\cdot\vec{u}^m}\rangle \langle e^{-i\vec{K}\cdot\vec{u}^{m'}}\rangle \right) . \quad (1)$$

Here $\vec{K}=\vec{k}-\vec{k}'$ is the scattering vector, $\vec{R}^m$ the position of atom m in the *ideal* lattice, and $\vec{u}^m$ the static displacement from this position. The first term in the bracket gives the total intensity, and we have subtracted the Bragg intensity (second term) to obtain the diffuse intensity alone.

The displacement $\vec{u}^m$ is a superposition of the displacements $\vec{t}^{\,m,n}$ due to defects at the different positions n. We introduce a random number $s^n = 1$ or 0, if the position n is occupied by a defect or not (e.g., impurity, vacancy or center of defect cluster, dislocation loop, etc.),

$$\vec{u}^m = \sum_n s^n \vec{t}^{\,m,n} . \quad (2)$$

Further, we assume that the different defects are not correlated, i.e., the numbers s^n and $s^{n'}$ are independently distributed. Then the averages in (1) can be calculated using the relations $(s^n)^2 = s^n$